JOURNAL OF APPLIED CRYSTALLOGRAPHY

ISSN 1600-5767

Received 9 May 2025
Accepted 24 July 2025

Edited by J. Ilavsky, Argonne National Laboratory, USA

Keywords: anomalous small-angle X-ray scattering; ASAXS; atomic scattering factors; X-ray absorption; data interpretation.

On the determination of resonant curves in anomalous small-angle X-ray scattering

Dragomir Tatchev,[a]* Armin Hoell,[b] Ruzha Harizanova[c] and Irena Mihailova[c]

[a]Institute of Physical Chemistry, Bulgarian Academy of Sciences, Acad. G. Bonchev Street Bl. 11, Sofia 1113, Bulgaria, [b]Helmholtz-Zentrum Berlin für Materialien und Energie, Hahn-Meitner-Platz 1, Berlin 14109, Germany, and [c]University of Chemical Technology and Metallurgy, 8 Kl. Ohridski Boulevard, Sofia 1756, Bulgaria. *Correspondence e-mail: dtachev@ipc.bas.bg

Data interpretation in anomalous small-angle X-ray scattering (ASAXS) relies on the atomic scattering factors of the resonant element near its X-ray absorption edge. The standard approach has been to use tabulated atomic scattering factors. However, these refer to free isolated atoms, while ASAXS typically probes condensed matter systems such as solids, liquids or soft matter. This discrepancy is addressed by measuring the X-ray absorption spectrum near the absorption edge and applying the Kramers–Kronig relations (Hilbert transform) to extract the atomic scattering factors of the resonant element. A related issue is the frequent occurrence of partially or fully negative resonant scattering curves, which is resolved by revisiting the assumptions of the data analysis. Two example experiments are presented to demonstrate our improved interpretation: ASAXS measurements of Xe physisorption in a nanoporous Si membrane near the Xe absorption edge, and the precipitation of magnetite/hematite in an Fe-doped soda-lime silicate glass.

1. Introduction

Anomalous small-angle X-ray scattering (ASAXS), developed mainly by Stuhrmann (1980, 1981, 1982, 1985) in the early 1980s, is a contrast-variation technique with numerous applications in materials science and molecular biology, as recently reviewed (Sun, 2021; Cheng *et al.*, 2023; Sakurai, 2017). The core principle of the method involves measurements at X-ray energies near the absorption edge of a specific chemical element within the sample. The resulting scattering curves vary with energy due to the anomalous dispersion associated with the absorption edge of this specific element.

The interpretation of ASAXS data can generally be approached in three ways: simultaneous fitting of all scattering curves using the same nanostructural model but varying contrasts, subtraction of two scattering curves in some special cases, or solving a system of three or more linear equations for multiple scattering curves. This last is often referred to as 'Stuhrmann's method', the 'scattering curve separation method' or 'partial structure factor determination'. Simultaneous model fitting of several scattering curves measured at different energies is typically performed using dedicated software, such as *SASfit* (Breßler *et al.*, 2015; Kohlbrecher & Breßler, 2022), but it requires prior knowledge of the nanostructure of the investigated object. The fitting procedure needs fixed structure parameters while only the scattering contrast changes with energy. The advantage is the significantly reduced likelihood of fitting the data with an incorrect multi-parameter model, though it does not eliminate the risk entirely.

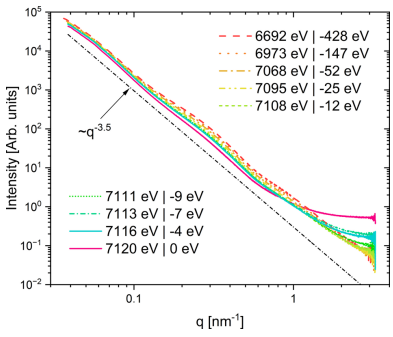

The other two methods are model free and aim to determine the 'resonant curve', which corresponds to a two-phase system composed of atoms of the resonant element in a vacuum. Once the resonant scattering curve is determined, its interpretation – whether qualitative or through model fitting – is decoupled from the influence of other constituents in the studied object. This is especially advantageous when the resonant element is confined to a single phase. In such cases, the resonant curve can be analysed using the full set of tools developed for two-phase systems.

Numerous studies have explored the determination of resonant scattering curves in small-angle scattering using both Stuhrmann's method and the two-curve difference method (Haas *et al.*, 2010; Hoell *et al.*, 2009; Haubold & Wang, 1995). Since the anomalous effect is often quite small, these approaches require precise measurement of the scattering curves and sample transmission, as well as accurate primary data reduction. Nevertheless, several challenges remain.

The most common issue when applying Stuhrmann's method is the appearance of partially or completely negative resonant scattering curves. Attempts to improve statistical reliability by overdetermining the linear system – *i.e.* measuring at more than three energies – often fail to resolve this issue. In fact, it is sometimes observed that selecting different triads of scattering curves yields varying positive resonant curves, while combining all measured curves (more than three) produces a negative result. This sensitivity of the resonant curve to the choice of energy points is problematic and may lead researchers to suspect measurement errors in some of the scattering curves.

The determination of the resonant scattering curve using Stuhrmann's method requires knowledge of the atomic scattering factors of the resonant element near its absorption edge. Theoretically calculated data for atomic scattering factors are available and commonly used (Henke *et al.*, 1993; Chantler, 2000; Cromer & Liberman, 1981). However, these tabulated values refer to free isolated atoms, whereas ASAXS typically investigates condensed matter – solids and liquids. In such systems, the absorption spectra exhibit oscillatory features known as near-edge X-ray absorption fine structure (NEXAFS or XANES) and extended X-ray absorption fine structure (EXAFS), which result from interactions between the ejected photoelectron and neighbouring atoms. Additionally, the absorption edge often exhibits a chemical shift depending on the chemical state of the resonant atom, and certain elements may show pre-edge peaks.

The standard procedure in ASAXS accounts for the chemical shift by simply shifting the corresponding tabulated atomic scattering factors. However, this approach neglects the finer structure of the absorption spectrum. Furthermore, the accuracy of the tabulated dispersion corrections, f' and f'', is limited in the near-edge region. Chantler (2000) provided uncertainty estimates for f' and f'', showing deviations of up to 30% within 10% of the K-edge energy. This level of uncertainty is problematic when analysing anomalous effects of the order of just a few per cent. Therefore, the reliability of the conventional procedure for determining the resonant curve remains questionable.

This contribution addresses the aforementioned issues by replacing the tabulated f'' data near the absorption edge with values derived from measured absorption spectra. The corresponding f' values are then calculated using the Kramers–Kronig relations. This approach does not require additional measurements, as absorption spectra near the target edge are already acquired as part of the ASAXS experiment.

Two ASAXS experiments are analysed as illustrative examples. In both cases, a strong anomalous effect was observed; however, attempts to determine the resonant scattering curve using Stuhrmann's method were partially or completely unsuccessful.

2. Theory

The model-free method for determining resonant scattering curves appears to have originated with Stuhrmann (1985). It is based on a curve separation scheme, which decomposes each scattering curve into a set of three contributions: resonant $I_{\rm R}(q)$, non-resonant $I_0(q)$ and a cross-term $I_{0\rm R}(q)$,

$$I(q,\varepsilon) = \left(f'^2 + f''^2\right) I_{\rm R}(q) + f' I'_{0\rm R}(q) + I_0(q). \tag{1}$$

f' and f'' are the real and imaginary corrections, respectively, to the atomic scattering factor near the X-ray absorption edge:

$$f(\varepsilon) = f_0 + f'(\varepsilon) + if''(\varepsilon). \tag{2}$$

ε represents the X-ray energy and q the magnitude of the scattering vector [$q = (4\pi/\lambda)\sin\theta$, where θ is half the scattering angle and λ is the wavelength of the incident radiation]. The corrections to the atomic scattering factors are typically taken from the aforementioned public sources (Chantler, 2000; Henke *et al.*, 1993). Thus, equation (1) enables the construction of a linear system of three equations for $I_{\rm R}(q)$, $I_0(q)$ and $I_{0\rm R}(q)$ at each value of q, by performing measurements at three different X-ray energies near the absorption edge of a chemical element present in the sample.

According to a recent review of ASAXS theory, an additional term in equation (1) proportional to f'' exists in the case of centrosymmetric or isotropic scattering media (Tatchev, 2008). The complete expression for a single-edge multi-atom system is as follows [see Tatchev (2008) for notations and further details]:

$$I(\mathbf{q},\varepsilon) = \left(f'^2 + f''^2\right) I_{\rm R1}(\mathbf{q}) + f'_1 I'_{0\rm R1}(\mathbf{q}) + f''_1 I''_{0\rm R1}(\mathbf{q}) + I_{01}(\mathbf{q}), \tag{3}$$

where

$$\begin{aligned} I_{\rm R1} &= S_{11}, \\ I'_{0\rm R1} &= 2\left\{ f_{01} S_{11} + \sum_{j=2}^{n} \left[\left(f_{0j} + f'_j\right) {\rm Re}\left(S_{1j}\right) + f''_j {\rm Im}\left(S_{1j}\right) \right] \right\}, \\ I''_{0\rm R1} &= 2\sum_{j=2}^{n} \left[f''_j {\rm Re}\left(S_{1j}\right) - \left(f_{0j} + f'_j\right) {\rm Im}\left(S_{1j}\right) \right] \end{aligned} \tag{4}$$

and I_{01} = I_0 + all remaining terms from equation (22) of Tatchev (2008).

Here the resonant element bears index 1. The imaginary part $\mathrm{Im}(S_{1j})$ of the cross-element partial structure factors is zero for centrosymmetric or isotropic media, but a term proportional to its real part $\mathrm{Re}(S_{1j})$ still remains and f_j'' for the non-resonant elements has to be set to zero for the $I''_{0\mathrm{R}1}$ to disappear. That is exactly the approximation Stuhrmann made at the beginning of his derivation of (1) – *e.g.* equation (20) of Stuhrmann (1985). However, tables of f' and f'' show that f'' may be small but does not equal zero, even far from absorption edges. Thus, for the example given below, f'' ranges between 0.81 and 0.96, but f' is between 0.37 and 0.39 for Si at energies near the Xe L_{III} absorption edge (Henke *et al.*, 1993).

Another possible curve separation scheme may be obtained by a different rearrangement of equation (22) of Tatchev (2008). With $f_{\mathrm{R}i}$ denoting the real part, $f_{0i} + f_i'$, of the atomic scattering factor it reads

$$I(\mathbf{q},\varepsilon) = \left(f_{\mathrm{R}1}^2 + f_1''^2\right) I_{\mathrm{R}1}(\mathbf{q}) + f_1' I'_{0\mathrm{R}1}(\mathbf{q}) + f_1'' I''_{0\mathrm{R}1}(\mathbf{q}) + I_{01}(\mathbf{q}), \tag{5}$$

where

$$\begin{aligned} I_{\mathrm{R}1} &= S_{11}, \\ I'_{0\mathrm{R}1} &= 2\sum_{j=2}^{n}\left[f_{\mathrm{R}j}\mathrm{Re}\left(S_{1j}\right) - f_j''\mathrm{Im}\left(S_{1j}\right)\right], \\ I''_{0\mathrm{R}1} &= 2\sum_{j=2}^{n}\left[f_j''\mathrm{Re}\left(S_{1j}\right) + f_{\mathrm{R}j}\mathrm{Im}\left(S_{1j}\right)\right] \end{aligned} \tag{6}$$

and I_{01} = all remaining terms with $i > 1$ from equation (22) of Tatchev (2008).

Again, the term proportional to f'' of the resonant atom will disappear if f'' for all non-resonant atoms is zero, and only for centrosymmetric or isotropic media for which $\mathrm{Im}(S_{1j}) = 0$. The latter separation scheme will obviously lead to a worse conditioned matrix since $f_{\mathrm{R}1} = f_{01} + f_1'$, where f_{0i} does not depend on the energy and is larger than both f_1' and f_1''. Nevertheless, the scheme is also operational and leads to the same results as equations (4).

In a series of reports, Goerigk and co-workers employed a curve separation scheme that appears similar to equation (5) but is instead derived from equation (70) of Tatchev (2008). As a result, it requires knowledge of the scattering contrasts, *i.e.* the composition of the scattering (thermodynamic) phases within the sample (Goerigk & Mattern, 2010; Goerigk & Williamson, 1998, 2001*a*, 2001*b*). The outcome is a resonant phase scattering function which corresponds to the partial scattering factor only if the resonant element is confined to a single phase.

3. Experimental

The sample under study was a soda-lime silicate glass with the composition $16Na_2O$–$10CaO$–$49SiO_2$–$25Fe_2O_{3-\delta}$, prepared using a conventional high-temperature melt-quenching technique. A 75 g batch of powdered raw materials (Na_2CO_3, SiO_2, $CaCO_3$ and $FeC_2O_4{\cdot}2H_2O$) was homogenized and then heated in a fused silica crucible from room temperature to 1400°C at a rate of 10°C min^{-1}. The melt was held at this temperature for 1 hour and then quenched into a graphite mould preheated to 450°C. Once the surface of the cast sample had solidified, it was transferred to a muffle annealing furnace. To reduce mechanical stresses, the sample was annealed at 450°C for 10 min. The furnace was then switched off and the sample was allowed to cool to room temperature at the natural furnace cooling rate (Harizanova *et al.*, 2024*a*).

From the resulting block, plane-parallel pieces with dimensions of 1 × 1 × 0.5 cm were cut. The top and bottom surfaces were removed by grinding, and the samples were annealed for 1 hour at 580°C to induce nanoparticle formation. The phase composition and microstructure after annealing were characterized using X-ray diffraction (XRD), transmission electron microscopy (TEM) (Harizanova *et al.*, 2024*a*) and computed tomography.

ASAXS measurements of the iron-containing glass near the Fe absorption edge were performed on the four-crystal monochromator beamline of the Physikalisch-Technische Bundesanstalt at the Helmholtz-Zentrum Berlin (HZB) synchrotron radiation facility BESSY II (Krumrey, 1998) using the HZB-ASAXS instrument. The sample absorption near the Fe *K* edge was measured on the same beamline in transmission mode using the ASAXS setup. Normalization of the absorption spectrum and linear fitting were performed using the *Athena* software package (Ravel & Newville, 2005). Magnetite (Fe_3O_4) and hematite (α-Fe_2O_3) were identified in the samples by X-ray diffraction, and the corresponding absorption spectra were retrieved from the IXAS X-ray Absorption Data Library (https://xaslib.xrayabsorption.org/elem/Fe).

Additionally, ASAXS measurements of xenon physisorption in a nanoporous silicon membrane near the Xe absorption edge were used, although the experimental details are omitted here as they have been published elsewhere (Gericke *et al.*, 2021).

The systems of linear equations used to determine the resonant scattering curve were solved using both singular value decomposition (SVD) and *QR* decomposition. The two methods yielded identical results. Column-wise matrix normalization was applied to improve the conditioning of the system.

All scattering curves were corrected for their individual constant background scattering prior to any further processing.

4. Results and discussion

4.1. ASAXS at the Xe L_{III} absorption edge

Xenon physisorption in nanoporous silicon appears to be an ideal candidate for ASAXS analysis. The system consists of two components and may form either a two-phase or a three-phase system, depending on the specific configuration. Under normal conditions, the porous medium is a two-phase system of a matrix with open porosity only, such that each pore can be filled with gaseous xenon.

Under pressure-induced physisorption, a third phase consisting of liquid xenon may form. In such a configuration, determination of the resonant scattering curve becomes meaningful. Given the extremely low electron density of gaseous xenon (mass density at boiling point 0.01 g cm^{-3}) compared with liquid xenon (mass density 2.94 g cm^{-3}), the resonant contribution in this case would predominantly arise from the physisorbed (liquid) xenon phase.

This case appears ideal for ASAXS: the resonant element is a chemically inert atomic gas and the tabulated dispersion corrections for the atomic scattering factor should accurately represent the system under investigation. Nevertheless, attempts to calculate the resonant scattering curve using data from five X-ray energies were unsuccessful. Various combinations of three energies out of the five were tested, each yielding different resonant curves. This inconsistency ultimately led to the exclusion of one of the five measurements from further analysis [see the supporting snformation for Gericke *et al.* (2021)].

All five ASAXS scattering curves measured near the Xe $L_{\rm III}$ absorption edge were used to determine the resonant scattering curve via equation (3). The anomalous effect is illustrated in the top panel of Fig. 1. The bottom panel shows the extracted Xe resonant scattering curve, along with the remaining three components described in equations (4), now expressed in the form

$$\begin{aligned} I_{\rm R1} &= S_{\rm XeXe}, \\ I'_{\rm 0R1} &= 2\left[f_{\rm 0Xe}S_{\rm XeXe} + \left(f_{\rm 0Si} + f'_{\rm Si}\right){\rm Re}\left(S_{\rm XeSi}\right)\right], \\ I''_{\rm 0R1} &= 2f''_{\rm Si}{\rm Re}\left(S_{\rm XeSi}\right), \\ I_{01} &= f^2_{\rm 0Xe}S_{\rm XeXe} + 2f_{\rm 0Xe}\left(f_{\rm 0Si} + f'_{\rm Si}\right){\rm Re}\left(S_{\rm XeSi}\right) \\ &\quad + \left[\left(f_{\rm 0Si} + f'_{\rm Si}\right)^2 + f''^2_{\rm Si}\right]S_{\rm SiSi}. \end{aligned} \tag{7}$$

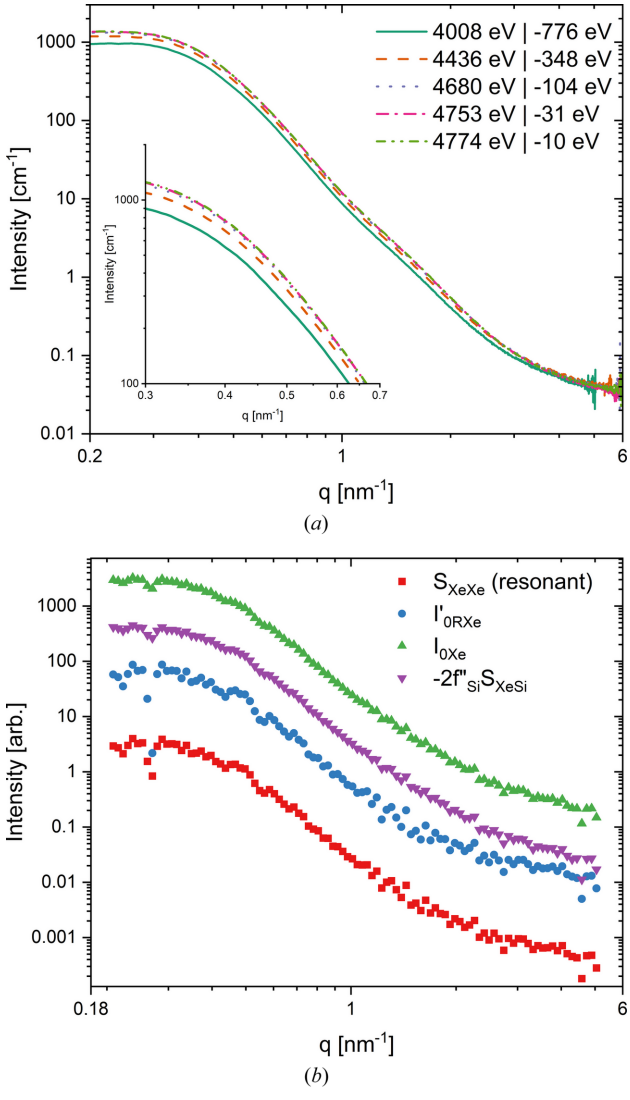

Figure 1
(*a*) ASAXS curves of Xe in mesoporous Si at a pressure of 650 mbar. The distance from the $L_{\rm III}$ absorption edge of Xe is given, together with the X-ray energies. (*b*) Calculated resonant curve together with all other terms of equation (5).

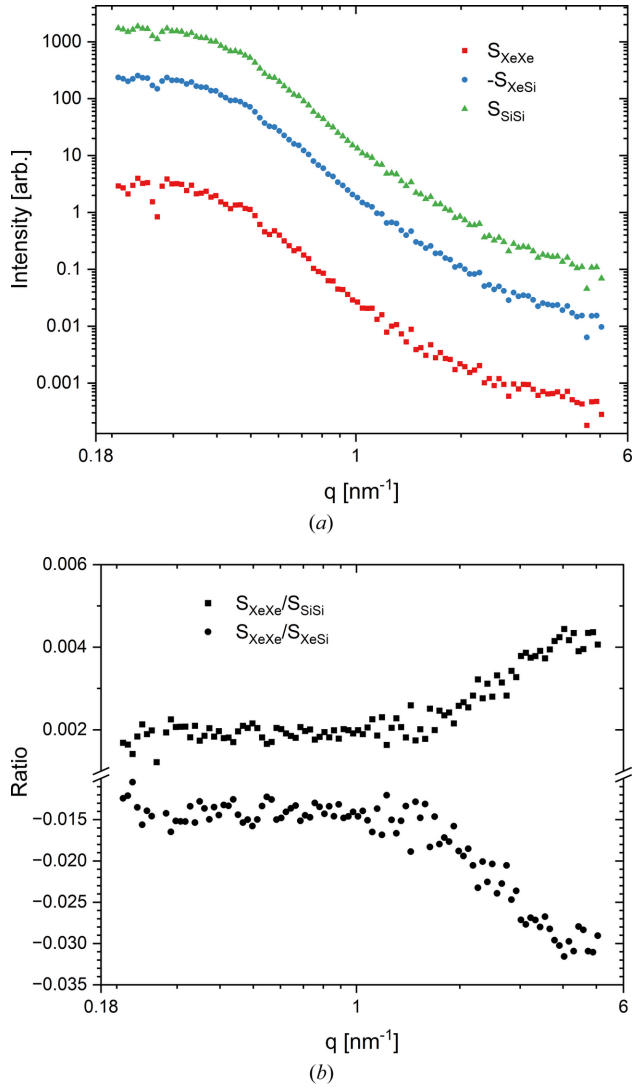

Figure 2
(*a*) All three partial structure factors for the two-component system. (*b*) Ratios of partial structure factors.

Obviously, equations (7) form a system for the three partial scattering functions S_{XeXe}, S_{XeSi} and S_{SiSi}. They can be calculated if we keep in mind that equations (3) and (4) are single-edge approximations and the energy dependence of f'_{Si} and f''_{Si} may be neglected, which allows us to replace them by the means, *e.g.* 0.38 and 0.88, respectively. The three partial scattering functions are shown in Fig. 2(*a*). Note that S_{XeSi} (I''_{0R1}) is negative. The ratios between partial structure functions are plotted in Fig. 2(*b*). They show that the partial structure factors are not proportional to each other. The system cannot be treated as a two-phase one – the pores are almost full of liquid Xe, but some small parts are still empty, giving a deviation of proportionality at $q > 1$ nm^{-1}.

Actually, seven scattering curves were measured during the experiment of Gericke: the five shown in Fig. 1(*a*) and two more at 4780 and 4782 eV. Attempts to include any of the last two with any combination of the other five resulted in negative resonant curves with only a few positive points. The most probable reason is the accuracy of the calculated atomic scattering factors near the edge, as discussed by Chantler (2000). The two incompatible energies are the closest to the absorption edge, −2 and −4 eV. Nevertheless, the proposed correction is already an improvement on Gericke's experiment, since it uses five instead of three energies and has a plausible explanation for skipping the scattering curves closest to the edge.

4.2. ASAXS at the Fe *K* absorption edge

XRD analysis of the as-quenched glass reveals an amorphous matrix containing crystalline inclusions of magnetite (Fe_3O_4) and hematite (α-Fe_2O_3) (Harizanova *et al.*, 2024*a*). Tomographic imaging identifies inhomogeneities in the form of large plate-like structures with an average thickness of approximately 8 µm and a total volume fraction of around 1%. TEM further shows the presence of magnetite nanoparticles, roughly spherical in shape, with an average size of about 10 nm and an uneven spatial distribution throughout the sample volume (Harizanova *et al.*, 2024*b*). On the basis of the overall chemical composition, the maximum volume fraction of magnetite that could theoretically precipitate is estimated at about 36%.

Given these characteristics, small-angle scattering is expected to arise from a population of spherical particles, superimposed on a Porod-law background due to scattering from the larger plate-like inhomogeneities. Although not all magnetite has precipitated, interparticle interference effects are plausible under these conditions.

Fig. 3 presents the sample's 'edge scan' as a normalized absorption spectrum, along with reference spectra for magnetite and hematite. The sample spectrum closely fits a linear combination of the two reference spectra, with a magnetite-to-hematite ratio of approximately 84:16. The absorption edge of the sample is located at an energy of E_0 = 7120 eV, consistent with the value for magnetite. A chemical shift of 8 eV is observed.

Fig. 4 displays the small-angle scattering curves recorded at nine energies near the chemically shifted Fe *K* absorption edge. The overall scattering behaviour aligns with expectations: the curves approximately follow a Porod law, albeit with a power of 3.5 rather than the classical value of 4. Additionally, noticeable curvature in the regions between 0.04 and 0.2 nm^{-1}, 0.2 and 0.7 nm^{-1}, and 0.7 and 2 nm^{-1} suggests the presence of multiple scattering entities. While the anomalous effect is relatively pronounced, it varies along the measured q range, which rules out a simple two-phase system interpretation.

The initial attempt to analyse the data was carried out using *SASFit*. A core–shell particle model, combined with a Porod

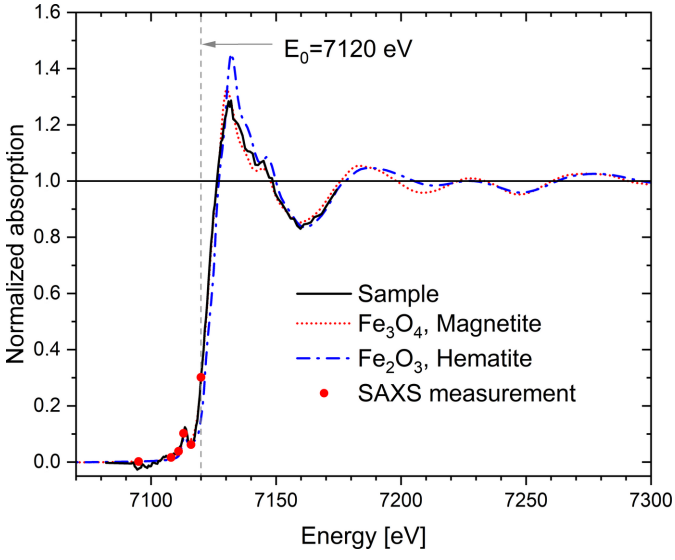

Figure 3
Normalized absorption spectrum of the investigated glass, together with those of magnetite and hematite. The energies at which SAXS curves were recorded are also indicated.

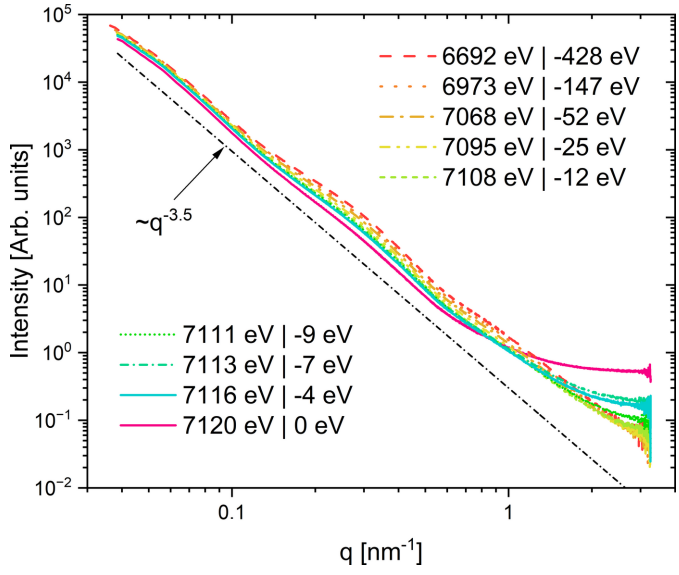

Figure 4
Scattering curves of the Fe-containing glass at nine energies near the shifted Fe *K* absorption edge.

background contribution, was successfully fitted to the scattering curves at 6692 and 7120 eV. Although the fits were satisfactory, some results were unexpected. Specifically, the Porod exponent was found to be 2.9, the average outer particle diameter – estimated at 60 nm – exceeded the values observed via TEM, and the derived core-to-glass scattering contrast appeared unreasonably low.

The resonant scattering curve I_R was obtained by solving the linear system of equation (1) using all nine ASAXS scattering curves (*i.e.* a system of nine equations with three unknowns). The values of f' and f'' were taken from the tables presented by Chantler (2000) with an applied chemical shift of 8 eV. The resulting resonant curve is shown in Fig. 5. I_R drops sharply to unphysical negative values below 0.2 nm^{-1}. This behaviour is inconsistent with expectations, especially considering that, as seen in Fig. 4, the anomalous effect – while decreasing at $q < 0.2$ nm^{-1} – remains substantial relative to other systems.

The use of equation (3) instead of (1) to construct a linear system of equations (this time nine equations and four unknowns) does not resolve the problem – the number of negative values of I_R decreases but is still large enough. Presumably, the use of f' and f'' for the free Fe atom is a problem since the absorption spectrum of the sample is quite different from that of a free Fe atom. Therefore, we should try to calculate relevant f' and f'' values with the help of the absorption spectrum of the sample.

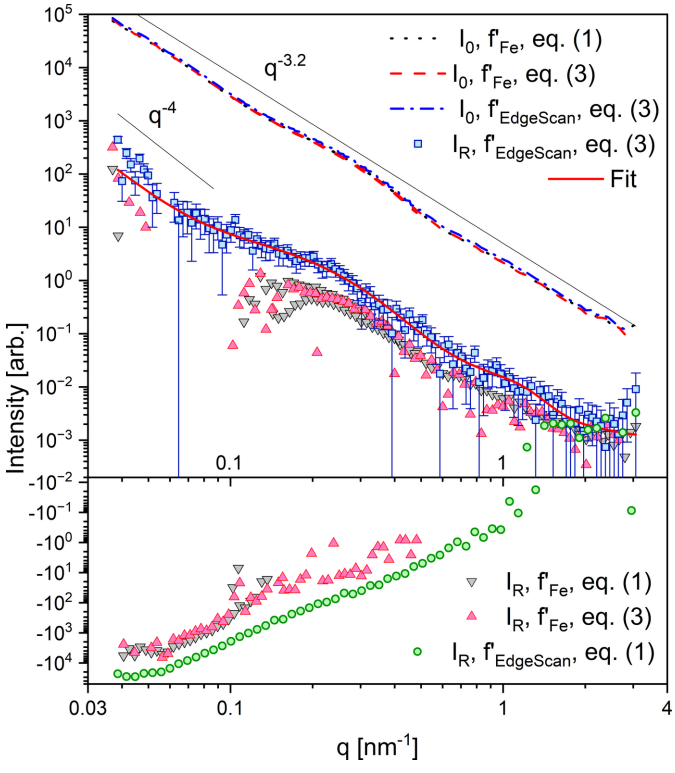

Figure 5
Resonant and non-resonant curves for Fe-containing glass calculated by equations (1) and (3), and with f' and f'' from tabulated data for a free Fe atom and calculated from the sample absorption spectrum.

The imaginary part f'' of the anomalous correction of the atomic scattering factors is directly connected to the cross section of photoelectric absorption (Stuhrmann, 1985; Henke *et al.*, 1993). Thus

$$f''(\varepsilon) = c\varepsilon\mu_{PE}(\varepsilon), \tag{8}$$

where $\mu_{PE}(\varepsilon)$ is the linear photoelectric absorption coefficient and c is a constant. The real correction, $f'(\varepsilon)$, is calculated from $f''(\varepsilon)$ by the Kramers–Kronig relations. Transmission measurements yield the total absorption coefficient of the sample. In this context, the contributions from incoherent (Compton) scattering and coherent (Rayleigh) scattering are small and can be reasonably neglected. For example, at 7112 eV, the respective mass attenuation cross sections are 0.068 cm^2 g^{-1} for Compton scattering and 1.745 cm^2 g^{-1} for

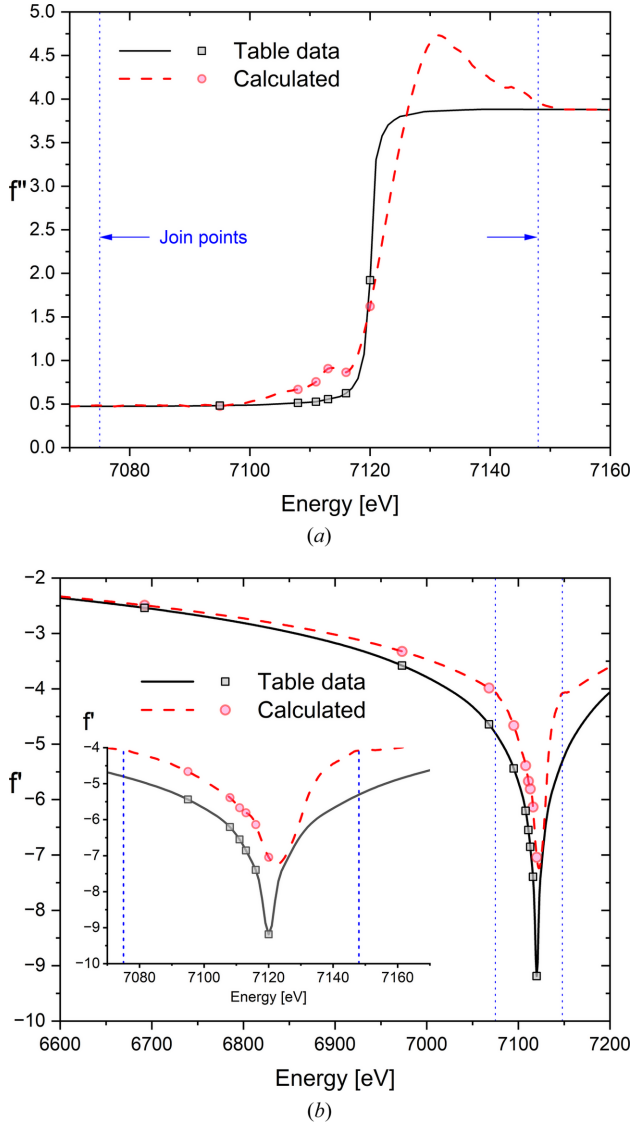

Figure 6
Anomalous dispersion corrections to the atomic scattering factors of Fe bonded in Fe_3O_4; the points correspond to values used for the coefficients of the linear system of equations (4) at the energies of the ASAXS curves. (*a*) Imaginary correction; (*b*) real correction.

Rayleigh scattering, in contrast to 51.38 $cm^2\ g^{-1}$ for photoelectric absorption (Berger *et al.*, 2010).

The application of the Kramers–Kronig relations needs a broader range of $f''(\varepsilon)$ to avoid deviations due to terminations at the ends. Thus, we took the tabulated data for $f''(\varepsilon)$ from 3 to 12 keV and replaced the part between 7075 and 7148 eV with $c\varepsilon\mu(\varepsilon)$ calculated from the measured absorption spectrum of the sample. The coefficient c was selected in such a way that the normalized absorption of 1 in Fig. 3 approximately matches the value of the tablulated data at the point of joining, 7148 eV. The resulting $f''(\varepsilon)$ near the Fe absorption edge is shown in Fig. 6. The Kramers–Kronig relations were applied to this $f''(\varepsilon)$ dependence.

The Kramers–Kronig relations are known in mathematics as the Hilbert transform. Numerical methods for calculating the Hilbert transform were developed a long time ago (Čížek, 1970; Marple, 1999) and functions for MATLAB (MATLAB Help Centre, https://www.mathworks.com/help/signal/ug/hilbert-transform.html) and Mathematica (Mangaldan, 2023; Costain & Çoruh, 2004) already exist. We used the code on p. 162 of Costain & Çoruh (2004) which gives a result identical to that of Mangaldan (2023). The mentioned routines are general purpose code used mainly in signal processing, so their output needs some scaling. The Hilbert transform was applied to the tabulated values of f'' for iron between 3 and 12 keV and the result was linearly scaled to coincide with the tabulated values of f'. The scaling coefficients were determined by a least-squares method, minimizing the difference just below the edge. Fig. 7 shows that f' calculated by the Hilbert transform coincides with the tabulated data from Chantler over a wide range below the absorption edge and sufficiently well within the edge. Therefore, the code of the Hilbert transform performs well enough for the purposes of this contribution.

Accordingly, the Hilbert transform was applied to the modified $f''(\varepsilon)$ and the resulting $f'(\varepsilon)$ is shown in Fig. 6(*b*). The calculated $f'(\varepsilon)$ curve is broader and less steep than the corresponding tabulated values for a free atom, which reflects the reduced sharpness of the experimental absorption edge, as illustrated in Fig. 6(*a*).

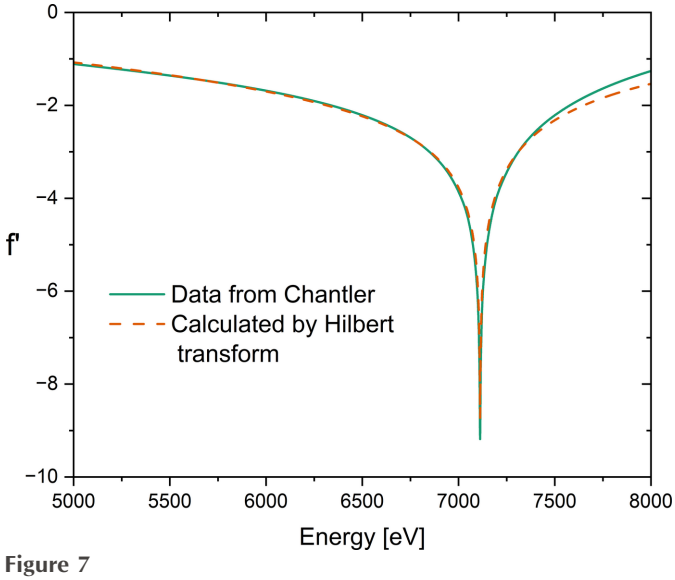

Figure 7
Plot of f' of Fe as given by Chantler (2000) and calculated by the Hilbert transform of f'' given by Chantler (2000).

Using the modified anomalous corrections for the atomic scattering factor of Fe in magnetite, we return to equation (3) to determine the four scattering contributions defined in equations (4). The data obtained at the two sample-to-detector distances were processed separately but are plotted using the same symbols in Fig. 5 to present a unified resonant scattering curve.

The resonant curve I_{R1} and the non-resonant one I_{01} are shown in Fig. 5. The resonant curve is positive throughout and reproduces the shape of the curve calculated via equation (1) for $q > 0.2$–$0.3\ nm^{-1}$, indicating that equation (1) may be applicable under certain conditions. The three non-resonant curves in Fig. 5 appear nearly identical to each other and resemble the measured scattering curves at the lowest photon energies. However, the shape of the resonant curve determined from equation (3) using the modified f' and f'' differs from both the non-resonant and original ASAXS curves. Notably, the slight curvature at the lowest angles has vanished and the slope now approaches −4, while the two humps are more distinctly shaped. This suggests the presence of regions within the glass with low Fe content contributing to the scattering at $q < 0.2\ nm^{-1}$. Such regions could correspond to Fe-depleted diffusion zones surrounding the larger magnetite/hematite plates.

The resonant curve of the glass–ceramic sample fits well to a model consisting of spherical particles with a log-normal size distribution, Porod law ($\sim q^{-4}$) scattering and a constant background. The average particle size obtained from the fit is 12 nm, which agrees with the TEM observations. This fit is also included in Fig. 5. The benefits of ASAXS over conventional SAXS, and particularly the advantages of extracting the resonant curve over direct model fitting, are now evident, despite the sample being less than ideal due to the presence of at least two iron-containing phases with differing shapes and sizes.

The uncertainties on the data points of the resonant curves are seldom reported in the literature, though they can be easily calculated through standard error propagation procedures. In the case of an overdetermined system of equations, *i.e.* more than three (four) ASAXS curves being analysed, the three or four curves of equations (2) and (3) are linear transformations of the scattering curves through the pseudo-inverse matrix of the system matrix in the SVD method. The system matrix is composed of f' and f'' and contains no uncertainty since the tabulated data for f' and f'' have no uncertainties. The errors in the resonant curve could be calculated solely by the errors in the ASAXS curves. These errors are small for most points of the resonant curve, increasing only at higher angles where the errors of the ASAXS curves are larger.

For the method proposed here, the system matrix is calculated from an experimental absorption spectrum with the help of the Hilbert transform. Although the absorption spectrum has its own errors, analytical error propagation for the Hilbert

transform is impossible or difficult. Nevertheless, computing the uncertainties is desirable in view of the expected bad conditioning of the system matrix. Therefore, a Monte Carlo approach was adopted – the absorption spectrum was treated as 'exact' and normally distributed errors of 1% were added to each data point. We generated 11 perturbed data sets, computed resonant curves for each, and took the mean and standard deviation. This resulted in errors that are too small at high scattering angles since the errors in the data of the ASAXS curves are not accounted for. Thus, the two error types were summed and are plotted in Fig. 5 as uncertainties of the mean curve.

An important step in the resonant curve calculation is the smoothing of f'' prior to applying the Hilbert transform. A running average over seven points, which equals 3.5 eV, was used in the just-described calculation. This smoothing suppresses experimental noise, avoiding unphysical negative scattering intensities – a limitation when using tabulated f' and f''. Such a result is to be expected, since the resonant curve depends more on the accuracy of the system matrix than on the ASAXS data. Therefore, careful and accurate absorption scanning around the absorption edge could be key to obtaining a high-quality resonant scattering curve.

To complete the discussion of possible approaches to resonant curve evaluation, it should be noted that applying equation (1) with the modified f' and f'' produces a result inferior to any of the three shown in Fig. 5. Therefore, the most effective method for constructing the system of linear equations is to use equation (3) in conjunction with the independently calculated modified f' and f'', as proposed here. This approach requires only minimal additional effort, since the edge scan – needed to determine the absorption edge position – is routinely performed prior to the ASAXS measurement.

The proposed procedure for modifying the imaginary correction to the atomic scattering factors of an element in a compound could probably be improved further. Currently, the two segments of the $f''(\varepsilon)$ function do not join perfectly, leading to a discontinuity in its first derivative. This issue is partially mitigated by applying a running average smoothing method across five neighbouring points, which also helps reduce noise originating from the experimentally measured absorption spectrum of the sample. Nevertheless, a small discontinuity or 'bang' in the resulting f' curve remains visible above the edge, as seen in Fig. 6. This might be further improved by enforcing derivative continuity at the joining point.

Additionally, the choice of the energy range to be replaced is somewhat arbitrary. While the result appears insensitive to the upper boundary as long as it exceeds 25 eV above the edge, it is much more sensitive to the position of the lower boundary. This sensitivity probably arises from the energy selection used for recording the ASAXS curves – all energy points lie below the edge, and the transition point lies between them. The influence of the upper boundary would increase if an energy above the edge were used in the experiment. That is not the usual case, however, so the absorption spectrum is not measured at length above the edge. A potential improvement would be to measure the absorption spectrum across an energy range that fully encompasses all ASAXS measurement points. Despite these limitations, the results presented here are sufficient to demonstrate the feasibility and validity of the proposed approach.

5. Conclusions

Calculating resonant scattering curves using the ASAXS method has proven to be a challenging task. In this study, we propose two modifications to the standard approach.

First, we suggest abandoning the assumption that dispersion corrections to the scattering factors of non-resonant elements in the sample are equal to zero. Thus, instead of recording scattering curves at a minimum of three X-ray energies and using equation (1), one should measure them at at least four X-ray energies and use either equation (3) or equation (5).

Second, for resonant elements bonded in condensed matter, we recommend a procedure for modifying the imaginary component of the scattering factor f'' in the vicinity of the absorption edge. Specifically, this involves replacing the tabulated data with values calculated from the absorption spectrum of the sample. Using the modified factor f'', the real component f' is then calculated by the Hilbert transform. A reliable determination of resonant scattering curves in ASAXS requires accurate measurement not only of the scattering curves but also of the sample's absorption spectrum.

By applying these two modifications, we have successfully calculated the resonant scattering curve of xenon physisorbed in nanoporous silicon using scattering curves measured at five X-ray energies, as well as the scattering curve of an iron-containing phase in glass using data measured at nine X-ray energies.

Acknowledgements

The authors thank the Physikalisch-Technische Bundesanstalt, the German National Metrology Institute, for allowing us the use of the FCM beamline at BESSYII to perform the ASAXS measurements.

Conflict of interest

There are no conflicts of interest.

Data availability

Data are available upon request.

Funding information

The authors are grateful for financial support from the Bulgarian National Science Fund (contract No. KP-06-N48/4) and the European Union–Next Generation EU, through the National Recovery and Resilience Plan of the Republic of Bulgaria (project No. BG-RRP-2.004-0002, BiOrgaMCT).

References

Berger, M. J., Hubbell, J. H., Seltzer, S. M., Chang, J., Coursey, J. S., Sukumar, R., Sukumar, R. & Olsen, K. (2010). NIST Standard Reference Database 8 (XGAM). NIST, Maryland, USA. https://www.nist.gov/pml/xcom-photon-cross-sections-database.

Breßler, I., Kohlbrecher, J. & Thünemann, A. F. (2015). *J. Appl. Cryst.* **48**, 1587–1598.

Chantler, C. T. (2000). *J. Phys. Chem. Ref. Data* **29**, 597–1056.

Cheng, W., Chen, Z., Wu, X., Wu, Z., Wang, X., Zhao, M., Liu, H., Jia, H., Wang, C., Wang, X., Wu, Z. & Xing, X. (2023). *Symmetry* **15**, 1034.

Čížek, Vá. (1970). *IEEE Trans. Audio Electroacoustics* **18**, 340–343.

Costain, J. K. & Çoruh, C. (2004). *Handbook of geophysical exploration*, Vol. 1, *Basic theory of exploration seismology*. Amsterdam: Elsevier.

Cromer, D. T. & Liberman, D. A. (1981). *Acta Cryst.* A**37**, 267–268.

Gericke, E., Wallacher, D., Wendt, R., Greco, G., Krumrey, M., Raoux, S., Hoell, A. & Mascotto, S. (2021). *J. Phys. Chem. Lett.* **12**, 4018–4023.

Goerigk, G. & Mattern, N. (2010). *J. Phys. Conf. Ser.* **247**, 012022.

Goerigk, G. & Williamson, D. L. (1998). *Solid State Commun.* **108**, 419–424.

Goerigk, G. & Williamson, D. L. (2001*a*). *J. Appl. Phys.* **90**, 5808–5811.

Goerigk, G. & Williamson, D. L. (2001*b*). *J. Non-Cryst. Solids* **281**, 181–188.

Haas, S., Zehl, G., Dorbandt, I., Manke, I., Bogdanoff, P., Fiechter, S. & Hoell, A. (2010). *J. Phys. Chem. C* **114**, 22375–22384.

Harizanova, R., Mihailova, I., Cherkezova-Zheleva, Z., Paneva, D., Georgieva, M., Tzankov, D., Avdeev, G. & Rüssel, C. (2024*a*). *Bol. Soc. Española Cerámica Vidrio* **63**, 23–32.

Harizanova, R., Mihailova, I., Georgieva, M., Tzankov, D., Cherkezova-Zheleva, Z., Paneva, D., Avramova, I., Karashanova, D., Avdeev, G., Gugov, I., Setzer, A., Esquinazi, P. & Rüssel, C. (2024*b*). *J. Non-Cryst. Solids* **634**, 122986.

Haubold, H. G. & Wang, X. H. (1995). *Nucl. Instrum. Methods Phys. Res. B* **97**, 50–54.

Henke, L. B., Gullikson, E. M. & Davis, J. C. (1993). *At. Data Nucl. Data Tables* **54**, 181–342.

Hoell, A., Tatchev, D., Haas, S., Haug, J. & Boesecke, P. (2009). *J. Appl. Cryst.* **42**, 323–325.

Kohlbrecher, J. & Breßler, I. (2022). *J. Appl. Cryst.* **55**, 1677–1688.

Krumrey, M. (1998). *J. Synchrotron Rad.* **5**, 6–9.

Mangaldan, J. (2023). *Wolfram function repository,* https://resources.wolframcloud.com/FunctionRepository/resources/DiscreteHilbertTransform/.

Marple, L. (1999). *IEEE Trans. Signal Process.* **47**, 2600–2603.

Ravel, B. & Newville, M. (2005). *J. Synchrotron Rad.* **12**, 537–541.

Sakurai, S. (2017). *Polym. Int.* **66**, 237–249.

Stuhrmann, H. B. (1980). *Acta Cryst.* A**36**, 996–1001.

Stuhrmann, H. B. (1981). *Q. Rev. Biophys.* **14**, 433–462.

Stuhrmann, H. B. (1982). *Makromol. Chem.* **183**, 2501–2514.

Stuhrmann, H. B. (1985). *Adv. Polym. Sci.* **67**, 123–163.

Sun, Y. (2021). *Trends Chem.* **3**, 1045–1060.

Tatchev, D. (2008). *Philos. Mag.* **88**, 1751–1772.